Site Preferences in the Mixed Cation Zeolite, Li,Na-Chabazite: A Combined Solid-State NMR and Neutron Diffraction Study

Luis J. Smith,[†,§] Hellmut Eckert,[‡] and Anthony K. Cheetham*[,†]

Contribution from the Materials Research Laboratory, University of California, Santa Barbara, California 93106, and Institut für Physikalische Chemie, Westfälische Wilhelms-Universität Münster, D-48149 Münster, Germany

Received August 9, 1999

Abstract: The locations of Li^+ and Na^+ cations in dehydrated chabazite were studied by neutron powder diffraction, ^{7}Li and ^{23}Na magic-angle spinning (MAS) nuclear magnetic resonance (NMR) spectroscopy, and ^{23}Na multiple quantum MAS (MQMAS) NMR spectroscopy. Neutron powder diffraction data were collected on lithium chabazite (space group: $R\bar{3}m$, $a = 9.3357(5)$ Å, $\alpha = 93.482(4)°$, $R_{wp} = 5.83\%$, $R_p = 4.65\%$, $\chi^2 = 1.24$) and on a mixed lithium sodium chabazite (space group: $R\bar{3}m$, $a = 9.3385(5)$ Å, $\alpha = 93.382(4)°$, $R_{wp} = 5.94\%$, $R_p = 4.83\%$, $\chi^2 = 1.27$). Both neutron diffraction and ^{7}Li MAS reveal lithium chabazite to have two cationic sites: one at the six-ring window of the hexagonal prism (SII) and one in the supercage at the four-ring window of the hexagonal prism (SIII). Mixed lithium−sodium chabazites reveal strong evidence of selective occupancy accompanied by concomitant rearrangement effects. While the introduction of sodium into lithium chabazite reduces occupation primarily at the SIII site, a decrease of the SII site lithium cation population is also observed at sodium levels above 24%. At low sodium content, sodium cations occupy a site in the eight-ring window of the channel (SIII′). At sodium content around 70% and higher, sodium cations also reside at the SII sites vacated by the lithium cations. The increased population of SII sites by Na^+ is associated with a marked increase in the lattice constant. The implications of the observed site preferences for noncryogenic air separation are discussed.

Introduction

Methods for the noncryogenic separation of oxygen and nitrogen from air have been developed since the 1970s and have led to a cost-effective process for this important separation.[1] These methods utilize adsorbents that exhibit an equilibrium or kinetic selectivity for one gas over the other. In the vacuum swing adsorption (VSA) process, absorbents that have nitrogen selectivity under equilibrium conditions are used. Lithium-containing zeolites have demonstrated good performance in such processes. Li-LSX, Li-X, and Li-Y, all members of the faujasite family, are common gas sorbents and have been previously studied.[2−5] In addition to the faujasites, lithium-containing chabazites have also demonstrated effective nitrogen sorption characteristics, making them potentially useful in VSA processes.[1] The separation effects are attributed to a strong interaction of the electric quadrupole moment of N_2 with the electrostatic field gradient created by the lithium cations.[6] For these reasons, recent work has been devoted to the structural characterization of the cation sites.[5,7] Despite this interest, little information exists on the structures of lithium-containing chabazites and the site preferences of extraframework cations.

Zeolites in the chabazite structural family have a three-dimensional channel system which contain pores made from an eight-membered ring of oxygen atoms. The channel structure results from the connection of hexagonal prisms by four-membered ring units. Cation sites in dehydrated and hydrated forms of natural chabazite have been previously studied and the resulting cation sites characterized.[8−12] From previous work three general cation positions are know to exist: one at the center of the prism, one at the six-ring window of the prism, and one at the eight-ring window (Figure 1). With a pore size of 3.8 Å, chabazite is a useful material for separations dealing with the passage of small molecules such as N_2 and light olefins.

While lithium-containing chabazite has been demonstrated to perform better in nitrogen sorption than other forms of chabazite, the lithium form does not have as great a hydrothermal stability as chabazites with cations of larger radius or higher charge. Mixed cation forms of chabazite, containing both lithium and another cation, can impart the greater thermal stability

* To whom correspondences should be addressed.
† University of California.
‡ Westfälische Wilhelms-Universität Münster.
§ Current address: Department of Chemistry, Purdue University, 1393 Brown Laboratories, West Lafayette, IN, 47907-1393.

(1) Gaffney, T. R. *Curr. Opin. Solid State and Mater. Sci.* **1996**, *1*, 69−75.
(2) Herden, H.; Einicke, W. D.; Schöllner, R.; Mortier, W. J.; Gellens, L. R.; Uytterhoeven, J. B. *Zeolites* **1982**, *2*, 131−134.
(3) Plévert, J.; Di Renzo, F.; Fajula, F.; Chiari, G. *J. Phys. Chem. B* **1997**, *101*, 10340−10346.
(4) Forano, C.; Slade, R. C. T.; Krogh Andersen, E.; Krogh Andersen, I. G.; Prince, E. *J. Solid State Chem.* **1989**, *82*, 95−102.
(5) Feuerstein, M.; Lobo, R. F. *Chem. Mater.* **1998**, *10*, 2197−2204.
(6) Pápai, I.; Goursot, A.; Fajula, F.; Plee, D.; Weber, J. *J. Phys. Chem.* **1995**, *99*, 12925−12932.
(7) Feuerstein, M.; Engelhardt, G.; McDaniel, P. L.; MacDougall, J. E.; Gaffney, T. R. *Microporous Mesoporous Mater.* **1998**, *26*, 27−35.
(8) Mortier, W. J.; Pluth, J. J.; Smith, J. V. *Mater. Res. Bull.* **1977**, *12*, 241−249.
(9) Mortier, W. J.; Pluth, J. J.; Smith, J. V. *Mater. Res. Bull.* **1977**, *12*, 97−102.
(10) Alberti, A.; Galli, E.; Vezzalini, G.; Passaglia, E.; Zanazzi, P. F. *Zeolites* **1982**, *2*, 303−309.
(11) Caligaris, M.; Mezzetti, A.; Nardin, G.; Randaccio, L. *Zeolites* **1984**, *4*, 323−328.
(12) Calligaris, M.; Mezzetti, A.; Nardin, G.; Randaccio, L. *Zeolites* **1986**, *6*, 137−141.

10.1021/ja992882b CCC: $19.00
Published on Web 02/08/2000

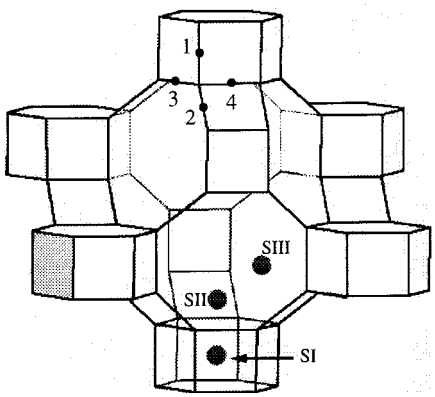

Figure 1. Representation of the extraframework cation positions in the hexagonal prism, SI, the six-ring window, SII, and the eight-ring window, SIII, of chabazite. The positions of the four unique oxygen atoms in the asymmetric unit are designated by atom number.

required while retaining lithium's superior adsorption properties.[1] In these mixed forms of chabazite, and other zeolites for that matter, the possibility exists for selective siting of the cations in the various positions. Accessibility of these extraframework cations will affect the sorption properties of the zeolite, and hence, manipulation of the site preferences of the cations can facilitate fine-tuning of the adsorption properties. Selective siting in mixed alkali LSX has recently been studied for this purpose.[7]

The challenge of characterizing extraframework cations in zeolites becomes more difficult when more than one cation serves to balance the negative charge of the zeolite framework. The occupancy of crystallographic positions can become too small to be measured accurately through powder diffraction. In addition, lighter cations such as lithium and sodium become difficult to locate with X-ray methods. While neutron powder diffraction, with its high sensitivity to light elements, has become the standard method for the crystallography of lithium-containing zeolites, it encounters limitations for sparsely populated sites such as those that may be present in mixed cation samples. However, solid-state nuclear magnetic resonance provides valuable complementary and quantitative information on the siting of extraframework cations in zeolites.

Past applications of both ^{7}Li and ^{23}Na MAS NMR experiments to zeolites have been able to identify distinct cation environments with varying degrees of resolution, despite the limited chemical shift ranges for the cationic forms of both nuclei. In ^{7}Li MAS NMR of faujasites, typically weakly coordinated noncage lithium cations (such as at the SIII site) have a lower resonance frequency than lithium coordinated in hexagonal prisms or six-rings.[5] ^{23}Na MAS NMR, too, can distinguish between cation environments, but the trends are not always as clearly resolved as in ^{7}Li NMR. The line shapes of ^{23}Na signals are broadened due to coupling of the large quadrupolar moment of sodium with the local electric field gradient of the cation environment. The broadening of the line shapes can make identification of individual sites difficult, and analysis becomes dependent on line shape simulation and fitting routines. While a hindrance for one-dimensional MAS experiments, the electric field gradient influencing the line shape depends on the local symmetry of the cation environment and provides an independent means of characterizing the cation site in addition to the chemical shift information. The recently developed multiple-quantum magic-angle spinning (MQMAS) technique,[13,14] which serves to produce isotropic spectra, allows for the determination of the nuclear electric quadrupolar coupling constants in an unambiguous way. The two-dimensional nature of the experiment often enables a line shape deconvolution of the different sites based on quadrupolar coupling and isotropic chemical shift, particularly in materials in which severe overlap of second-order quadrupolar line shapes exists.

The characterization of the local cation environment and the possible site preferences in mixed lithium−sodium chabazites are the subject of this study. Taking advantage of the benefits of both neutron powder diffraction and high resolution solid state NMR, chabazite samples with varying ratios of sodium and lithium cations are studied. Powder neutron diffraction data were collected for a fully lithiated sample and a mixed composition (58% Li, 42% Na). ^{7}Li MAS, ^{23}Na MAS, and ^{23}Na MQMAS NMR spectra were collected for a wider range of sodium/lithium ratios. Our results demonstrate that the cations in these mixed-akali chabazites exhibit definite site preferences: lithium cations prefer coordination at the six-ring window of the hexagonal prism, while sodium cations are preferentially directed toward the eight-ring window site.

Experimental Section

Sample Preparation. The potassium form of chabazite was synthesized from the decomposition of the acid form of zeolite Y. The sodium form of zeolite Y was ion-exchanged with a 1 M NH_4Cl aqueous solution using a solution-to-zeolite ratio of 50 mL/g in four exchange cycles. The ammonium form was calcined at 450 °C in air to produce the acid form. The acid form of zeolite Y was then mixed with 6 M KOH and Ludox (LS-30) and placed in a 95 °C oven for 7 days.[15] The resulting potassium chabazite was collected by filtration.

The as-synthesized zeolite was ion-exchanged to the sodium form using 1 M NaCl aqueous solution at a solution-to-zeolite ratio of 50 mL/g in eight to 10 exchange cycles each lasting 6−8 h in duration. Subsequently the lithium form of chabazite was produced from eight to ten ion-exchange cycles each 6−8 h in duration using 1 M LiCl aqueous solutions at 100 °C using the same solution-to-zeolite ratio. After each ion-exchange the sample was collected via filtration and subsequently washed with deionized water using 2−3 times the ion-exchange volume. Mixed alkali forms of chabazite were produced by ion-exchanging stoichiometric amounts of the appropriate chloride with the conjugate 100% form of chabazite using only one exchange cycle. The actual cation ratios produced were verified through elemental analysis using inductively coupled plasma (ICP) spectroscopy and are listed in Supporting Information. No significant cation deficiencies are evident within the error of the method. Eight samples were produced having the following lithium-to-sodium ratios: 100% Li, 86% Li:14% Na, 76% Li:24% Na, 61% Li:39% Na, 58% Li:42% Na, 20% Li:80% Na, 9% Li:91% Na, 100% Na. The silicon-to-aluminum ratio for the precursor zeolite and various samples after ion-exchange was determined to be 2.4 through both ICP and ^{29}Si NMR spectroscopy. All the zeolite samples were dehydrated under vacuum (5×10^{-5} Torr) at 500 °C and subsequently stored in an argon drybox where all samples were packed into MAS rotors for NMR experiments. ^{27}Al MAS NMR experiments were carried out on the dehydrated samples; no octahedral aluminum species were observed. Samples used in neutron diffraction were transferred to a helium drybox for loading into vanadium canisters.

Powder Diffraction. Neutron powder diffraction data on a 100% Li chabazite zeolite, a 58% Li:42% Na chabazite zeolite, and a 100% Na chabazite were collected at 295 K with a neutron wavelength of 2.083 Å between 8° and 150° in 2θ on the BT1 diffractometer at the National Institute of Standards and Technology (NIST). The structures of the fully lithiated chabazite and the mixed-alkali chabazite were refined using the Rietveld method[16] with the GSAS suite of programs.[17]

(13) Frydman, L.; Harwood, J. S. *J. Am. Chem. Soc.* **1995**, *117*, 5367−5368.
(14) Medek, A.; Harwood, J. S.; Frydman, L. *J. Am. Chem. Soc.* **1995**, *117*, 12779−12787.
(15) Bourgogne, M.; Guth, J.-L.; Wey, R., U.S. Patent 4,503,024, 1985.
(16) Rietveld, H. M. *J. Appl. Crystallogr.* **1969**, *2*, 65.

Table 1. Lattice Constants and Volumes of the Unit Cells for Lithium Chabazite, Mixed Sodium−Lithium Chabazite, and Sodium Chabazite Samples

sample	*a* (Å)	α (deg.)	volume (Å^3)	source
100% Li CHA	9.3357 (5)	93.482 (4)	808.7 (7)	neutron
76% Li: 24% Na CHA	9.3369 (15)	93.452 (1)	809.1 (4)	X-ray
58% Li: 42% Na CHA	9.3385 (5)	93.382 (4)	809.7 (6)	neutron
20% Li: 80% Na CHA	9.3423 (41)	92.694 (1)	812.4 (11)	X-ray
9% Li: 91% Na CHA	9.3536 (33)	92.731 (1)	815.2 (9)	X-ray
100% Na CHA	9.3716 (10)	92.643 (1)	820.2 (3)	neutron

A pseudo-Voigt profile function[18] with a Finger-Cox-Jephcoat asymmetry correction[19] was used to model the peaks. The background was fitted using a shifted-Chebyshev function. The diffraction data were refined in the $R\bar{3}m$ space group, using the rhombohedral setting, and the preliminary positions of the framework atoms were taken from the structure of dehydrated calcium chabazite.[9] The silicon and aluminum atoms were set to reside at the same crystallographic positions using occupancy ratios based on elemental analysis and ^{29}Si NMR. The cation positions were determined using difference Fourier maps. The thermal parameters for the framework atoms were refined and those for the extraframework cations were refined when possible and otherwise were fixed according to literature values.[3,20] The thermal parameters for the different lithium cations were constrained to be the same when refinement was possible. The diffraction data for the pure sodium chabazite was analyzed using the Le Bail method[21] to obtain lattice constants for the unit cell (Table 1). A full refinement of the structure was not possible due to the presence to two phases, one monoclinic and one rhombohedral, which caused the data collected to be underdetermined.

X-ray diffraction patterns were collected on three mixed-alkali samples: 76% Li:24% Na chabazite, 20% Li:80% Na chabazite, and 9% Li:91% Na chabazite at 295 K with a Scintag PAD-V powder diffractometer (45 kV, 35 mA) using Cu Kα1 and Kα2 radiation. The diffraction pattern for the samples was analyzed using a cell constant determination routine provided with the Scintag software (Table 1).

NMR Spectroscopy. ^{7}Li and ^{23}Na NMR experiments were performed on a Bruker Avance DSX-500 spectrometer with ^{7}Li and ^{23}Na resonance frequencies of 194.37 and 132.29 MHz respectively. For both MAS and MQMAS experiments, a Bruker 4 mm high-speed MAS probe modified for providing extra-high B_1-field amplitudes was used. One-dimensional ^{7}Li MAS spectra were acquired with a pulse length of 1.0 μs at a nutation frequency of 56 kHz for LiCl (aqueous). The spinning rate was 12 kHz and a recycle delay of 500 ms was employed. Under these conditions, rigorously quantitative spectra were recorded allowing reliable site populations to be obtained. Chemical shifts are reported relative to a 1 M LiCl solution as a reference standard. The one-dimensional ^{23}Na MAS experiments were performed at a spinning speed of 15 kHz using a 0.5 μs pulse at a nutation frequency of 114 kHz for NaCl (aqueous) with a recycle delay of 500 ms for all samples. The MAS spectra were fitted using the deconvolution routine from the xedplot program in the XWIN NMR suite of programs for the Bruker spectrometer. The intensities for the fit of the second-order quadrupolar broadened lines were adjusted according to the technique described by Massiot et al.[22] in order to obtain the correct cation populations from each line.

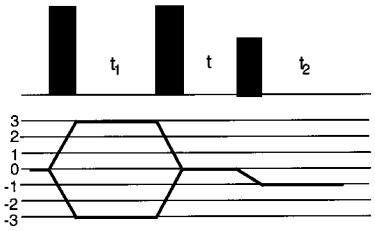

Figure 2. A schematic depiction of the MQMAS pulse sequence. A coherence transfer pathway diagram (bottom) describes the effects of each of the three pulses.

The two-dimensional ^{23}Na MQMAS experiments were carried out using the three-pulse zero-quantum filter sequence developed by Amoureux and co-workers[23] (Figure 2). The first and second pulses were hard pulses using a nutation frequency of 250 kHz for NaCl (aq) and had pulse lengths of 2 μs and 0.8 μs, respectively. The third pulse was a soft 90° pulse of 8.4 μs in length (nutation frequency of 32 kHz). The increments of the t_1 period, the delay between the first and second pulse, were typically 20 μs. A fixed delay of 10 μs was used between the second and third pulse. The spectra typically were collected with 64−128 different t_1 periods. Signals from the echo and antiecho were separated using the States method.[24] A recycle delay of 500 ms was employed and 800−1400 scans were collected per row. The resulting two-dimensional data set was Fourier transformed and sheared according to the method described by Massiot et al.[25] However, in addition to scaling the dwell time in the F_1 (isotropic) dimension and the offset in the isotropic dimension, the spectrometer frequency in the isotropic dimension was multiplied by the factor $(k + 3)/(1 + k)$.[26] For quadrupolar nuclei with a spin of $^3/_2$, k has a value of $^7/_9$. Scaling the isotropic dimension in this fashion serves to separate distributions in the chemical shifts and quadrupolar couplings by distinct slopes in the transformed spectra. All ^{23}Na chemical shifts are reported relative to a 1 M aqueous NaCl solution reference standard.

Isotropic chemical shift and quadrupolar product ($P_q = C_Q\,(1 + \eta^2/3)^{1/2}$) information can be obtained from these MQMAS spectra. The peaks in the MQMAS spectra have positions based on the following relationships:

$$\delta_{F_1} = \delta_{cs} + \frac{P_q^2 \times 10^6}{68\nu_o^2} \tag{1}$$

$$\delta_{F_2} = \delta_{cs} - \frac{P_q^2 \times 10^6}{40\nu_o^2} \tag{2}$$

The first moment of the peak in the second dimension is used since the fourth rank terms are zero at the center of mass of the line.[14] From these equations, it is clear that distributions of isotropic chemical shifts with a similar quadrupolar product will have a slope of 1. Distributions of the quadrupolar product for resonances with the same or similar isotropic chemical shift will have a slope of −10/17. The isotropic chemical shift and quadrupolar product are calculated using the following relationships:

$$\delta_{cs} = \frac{10}{27}\langle\delta_{F_2}\rangle + \frac{17}{27}\langle\delta_{F_1}\rangle \tag{3}$$

$$P_q = \sqrt{\frac{680\nu_o^2 \times 10^6}{27}(\langle\delta_{F_1}\rangle - \langle\delta_{F_2}\rangle)} \tag{4}$$

Results

Neutron Diffraction. The results of the refinement of the lithium chabazite structure are shown in Figure 3a, and the

(17) Larson, A. C.; Von Dreele, R. B. *Los Alamos Lab. Rep.* **1987**, *No. LA-UR-86-748*.
(18) Thompson, P.; Cox, D. E.; Hastings, J. B. *J. Appl. Crystallogr*. **1987**, *20*, 79−83.
(19) Finger, L. W.; Cox, D. E.; Jephcoat, A. P. *J. Appl. Crystallogr*. **1994**, *27*, 892−900.
(20) Olson, D. H. *Zeolites* **1995**, *15*, 439−443.
(21) Le Bail, A.; Duroy, H.; Fourquet, J. L. *Mater. Res. Bull.* **1988**, *23*, 447−452.
(22) Massiot, D.; Bessada, C.; Coutures, J. P.; Taulelle, F. *J. Magn. Reson.* **1990**, *90*, 231−242.
(23) Amoureux, J.-P.; Fernandez, C.; Steuernagel, S. *J. Magn. Reson. A* **1996**, *123*, 116−118.
(24) Ernst, R. R.; Bodenhausen, G.; Wokaun, A. *Principles of Nuclear Magnetic Resonance in One and Two Dimensions*; Clarendon: Oxford, 1987.

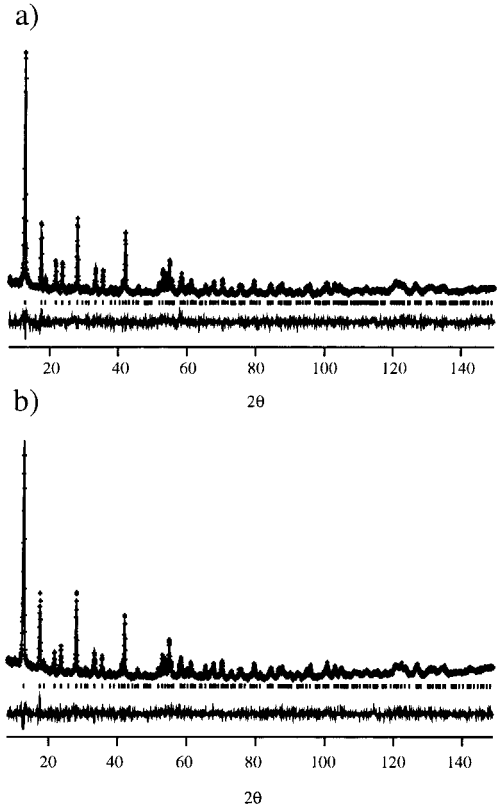

Figure 3. Final observed, calculated and difference profile plots for the neutron refinement of (a) lithium chabazite and (b) mixed sodium−lithium chabazite.

Table 2. Fractional Coordinates and U_{Iso} (isotropic thermal parameters) for Lithium Chabazite[a]

atom	site	*x*/*a*	*y*/*b*	*z*/*c*	occupancy	U_{iso} (Å^2)
Si(1)	12i	0.5968(11)	0.8242(9)	0.3748(10)	0.706	0.0250(22)
Al(1)	12i	0.5968(11)	0.8242(9)	0.3748(10)	0.294	0.0250(22)
O(1)	6g	0.7668(6)	0.2332(6)	0.5000	1.000	0.0276(26)
O(2)	6f	0.6205(6)	0.3795(6)	0.0000	1.000	0.0318(27)
O(3)	6h	0.7609 8)	0.7609(8)	0.3807(9)	1.000	0.0370(27)
O(4)	6h	0.5264(7)	0.5264(7)	0.7732(8)	1.000	0.0271(24)
Li(1)	2c	0.3718(23)	0.3718(23)	0.3718(23)	0.976(58)	0.0197(126)
Li(2)	12i	0.854(10)	0.309(11)	0.194(13)	0.132(10)	0.0197(126)

[a] Numbers in parentheses are standard errors in the last digit or digits.

positional parameters and occupancies are shown in Table 2. Bond lengths and angles are listed in Supporting Information. The final structure showed good agreement with the experimental data (R_p = 4.65%, R_{wp} = 5.83%, χ^2 = 1.24). The resulting structural model contained two distinct lithium sites: one in the center of the six-ring window, the SII site, and one in the corner of the four-ring window of the hexagonal prism, the SIII site (Figure 4a). No lithium cations were located inside the hexagonal prism or in the eight-ring window of the framework. The SIII lithium cation has a bond distance of 2.02 Å to the nearest oxygen, O(1). The next nearest coordinating oxygen is O(3) from the six-ring window at a distance of 2.32 Å (Figure 4a). The occupancy of the SII site is nearly 100% with 1.95 ± 0.12 cations per unit cell. At the SIII site, the cation population is 1.58 ± 0.12 cations per unit cell. Complete occupation of the SII site can also be inferred from the perturbations of the nearest oxygen atom, O(4). The T−O(4)

(25) Massiot, D.; Touzo, B.; Trumeau, D.; Coutures, J. P.; Virlet, J.; Florian, P.; Grandinetti, P. J. *Solid State Nucl. Magn. Reson.* **1996**, *6*, 73−83.

(26) Fernandez, C.; Amoureux, J. P.; Chezeau, J. M.; Delmotte, L.; Kessler, H. *Microporous Mater.* **1996**, *6*, 331−340.

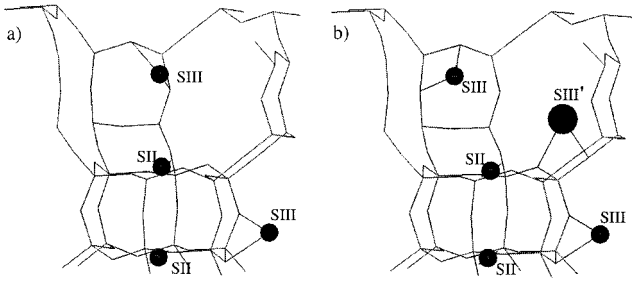

Figure 4. A stick representation of the structure of (a) dehydrated lithium chabazite and (b) dehydrated mixed sodium−lithium chabazite. The figures depict the lithium and sodium cations as spheres. Bonds are drawn to the SIII lithium site and to the SIII′ sodium site as guides for the eye. The tetrahedral and framework oxygen atoms are omitted for clarity.

Table 3. Fractional Coordinates and U_{Iso} (Isotropic Thermal Parameters) for Mixed Sodium−Lithium Chabazite[a]

atom	site	*x*/*a*	*y*/*b*	*z*/*c*	occupancy	U_{iso}(Å^2)
Si(1)	12i	0.6000(10)	0.8251(8)	0.3775(9)	0.706	0.0216(20)
Al(1)	12i	0.6000(10)	0.8251(8)	0.3775(9)	0.294	0.0216(20)
O(1)	6g	0.7654(5)	0.2346(5)	0.5000	1.000	0.0261(25)
O(2)	6f	0.6216(6)	0.3784(6)	0.0000	1.000	0.0348(26)
O(3)	6h	0.7594(7)	0.7594(7)	0.3797(9)	1.000	0.0330(25)
O(4)	6h	0.5253(6)	0.5253(6)	0.7728(8)	1.000	0.0276(24)
Li(1)	2c	0.3762(27)	0.3762(27)	0.3762(27)	0.841(45)	0.0210
Li(2)	12i	0.854	0.309	0.194	0.031(8)	0.0410
Na(1)	12i	0.016(9)	0.531(8)	0.144(9)	0.134(8)	0.0640

[a] Numbers in parentheses are standard errors in the last digit or digits.

bond length is the longest of the four bonds and the T−O(4)−T angle is the smallest. Both perturbations are the result attraction of the positive charge of the lithium cation pulling the oxygen atom closer to the SII site.

The mixed alkali (58% Li:42% Na) chabazite refinement is shown in Figure 3b and its positional and occupancy data are summarized in Table 3. Bond lengths and angles are listed in Supporting Information. Again the refinement was in good agreement with the experimental data (R_p = 4.80%, R_{wp} = 5.94%, χ^2 = 1.27). The structural model contains two extraframework lithium cation sites; only one sodium cation site is observed. The lithium cations are found in the SII and SIII sites as described in the structure for the full lithium sample. Due to the low occupancy of the SIII lithium site, the position of the lithium cation was constrained to be the same as that in the pure lithium chabazite. The sodium cation is found near the eight-ring window just outside of the plane of the window; the site will be henceforth referred to as the SIII′ site (Figure 4b). The sodium cation is at a distance of 2.32 Å from the O(3) oxygen atom of the six-ring window and 2.32 Å from the O(2) oxygen. The sodium occupancy is 1.61 ± 0.10 cations per unit cell. The occupancy of the SII lithium site was found to be incomplete, yielding 1.68 ± 0.09 cations per unit cell, while the occupancy of the SIII lithium site is 0.37 ± 0.10 cations per unit cell. Again the effect of the near total occupation of the SII site by lithium cations perturbs the length and angle of the T−O(4) bond.

NMR Spectroscopy. Figure 5 summarizes the ^{7}Li and ^{23}Na NMR data obtained on the whole suite of samples. The ^{7}Li MAS NMR spectrum of the fully lithiated chabazite consists of two peaks, one at −0.37 ppm and one at −1.22 ppm. The high-frequency peak has the larger area (63%) of the two peaks and is thus assigned to the SII site. Each ^{7}Li resonance is accompanied by a spinning sideband manifold arising from the effect of MAS on the first-order quadrupolar satellite transitions.

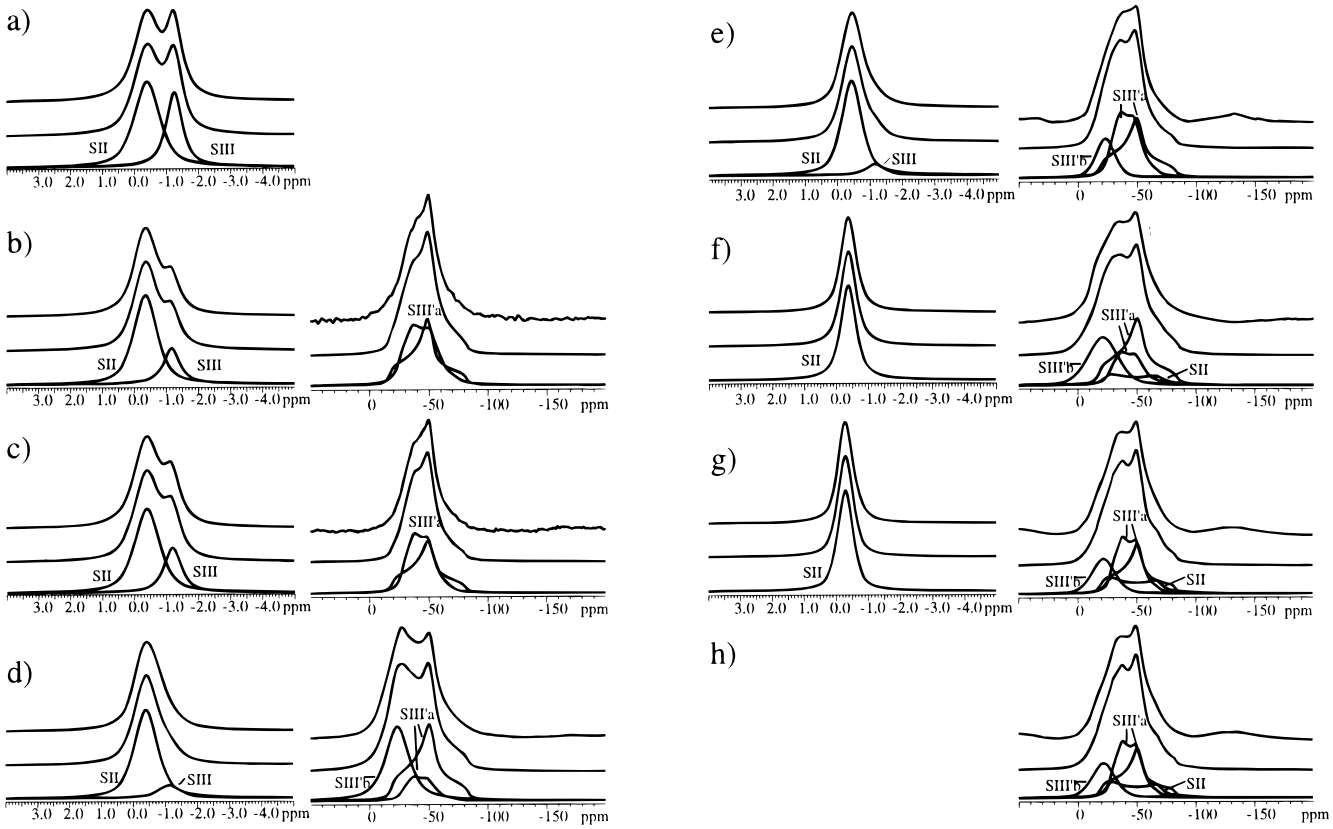

Figure 5. ^{7}Li MAS NMR (left) and ^{23}Na MAS NMR (right) spectra of chabazite with various cation contents: (a) 100% Li, (b) 86% Li:14% Na, (c) 76% Li:24%Na, (d) 61% Li:39% Na, (e) 58% Li:42% Na, (f) 20% Li:80% Na, (g) 9% Li:91% Na, and (h) 100% Na. The experimental spectrum is shown in the upper trace, the simulated in the middle, and the components of the simulation at the bottom.

Both sideband patterns can be separated by subtraction of the lower lithium content spectra from the spectra of the fully lithiated sample. The NMR spectra of the sideband patterns of the resonances are available in Supporting Information. The sideband patterns were found to yield consistent results despite the different levels of sodium present in each sample. As previously shown, the nuclear electric quadrupolar coupling parameters can be estimated from the overall envelopes of these sideband patterns.[27] The SII resonance is characterized by a quadrupolar coupling constant of 280 kHz with an $\eta \approx 0.3$. The SIII resonance has a quadrupolar coupling constant of 240 kHz with an $\eta \approx 1.0$. Thus, the ^{7}Li quadrupolar interaction parameters for both sites are clearly differentiable.

Figure 5 reveals that with increasing sodium content, the intensity of the minority lithium SIII peak decreases almost exclusively, indicating selective replacement by Na^{+}. Only at 39% sodium content does the intensity of the SII peak begin to decrease as well. The spectra of samples with higher sodium content levels contain only the peak at around −0.37 ppm. The shifts and areas for the ^{7}Li spectra are summarized in Table 4.

From Figure 5, it is clear that the ^{23}Na MAS spectra are rather broad and ill-defined, making assignments of the central transitions difficult without additional information regarding the chemical shifts and quadrupolar coupling constants of the sodium cations. MQMAS spectra provide the necessary information on the starting parameters for the MAS simulations. The ^{23}Na MQMAS spectrum of the 24% sodium sample, shown in Figure 6a, reveals only one type of sodium species. With the further addition of sodium, a second species becomes evident in the spectrum of the 39% sodium chabazite (Figure 6b). The corresponding 2-D contour remains sloped even after shearing, indicating the effect of a chemical shift distribution. As discussed further below, the additional feature is attributed to a second type of SIII′ site created by the cation disordering (SIII′b). In the spectrum of the 80% sodium chabazite (Figure 6c), the previous two species are present, and a third species is evident with a higher isotropic shift (∼10 ppm) and a larger nuclear electric quadrupolar coupling constant. The 100% sodium chabazite MQMAS spectrum (Figure 6d) reveals all three of these species with slightly higher intensities. The deconvolutions

Table 4. ^{7}Li MAS NMR Simulation Parameters and Site Populations of the Various Chabazite Samples

	SII	SIII	total
100% Li			3.53
δ_{iso} (ppm) (±0.07)	−0.37	−1.22	
Li^{+}/u.c.	2.22	1.31	
86% Li:14% Na			
δ_{iso} (ppm) (±0.07)	−0.36	−1.16	3.04
Li^{+}/u.c.	2.19	0.85	
76% Li:24% Na			
δ_{iso} (ppm) (±0.07)	−0.34	−1.18	2.68
Li^{+}/u.c.	2.01	0.67	
61% Li:39% Na			
δ_{iso} (ppm) (±0.07)	−0.38	−1.10	2.15
Li^{+}/u.c.	1.88	0.27	
58% Li:42% Na			
δ_{iso} (ppm) (±0.07)	−0.43	−1.16	2.05
Li^{+}/u.c.	1.85	0.20	
20% Li: 80% Na			
δ_{iso} (ppm) (±0.07)	−0.35	−	0.71
Li^{+}/u.c.	0.71	0	
9% Li: 91% Na			
δ_{iso} (ppm) (±0.07)	−0.28	−	0.32
Li^{+}/u.c.	0.32	0	

(27) Nielsen, N. C.; Bildsøe, H.; Jakobsen, H. J.; Norby, P. *Zeolites* **1991**, *11*, 622−632.

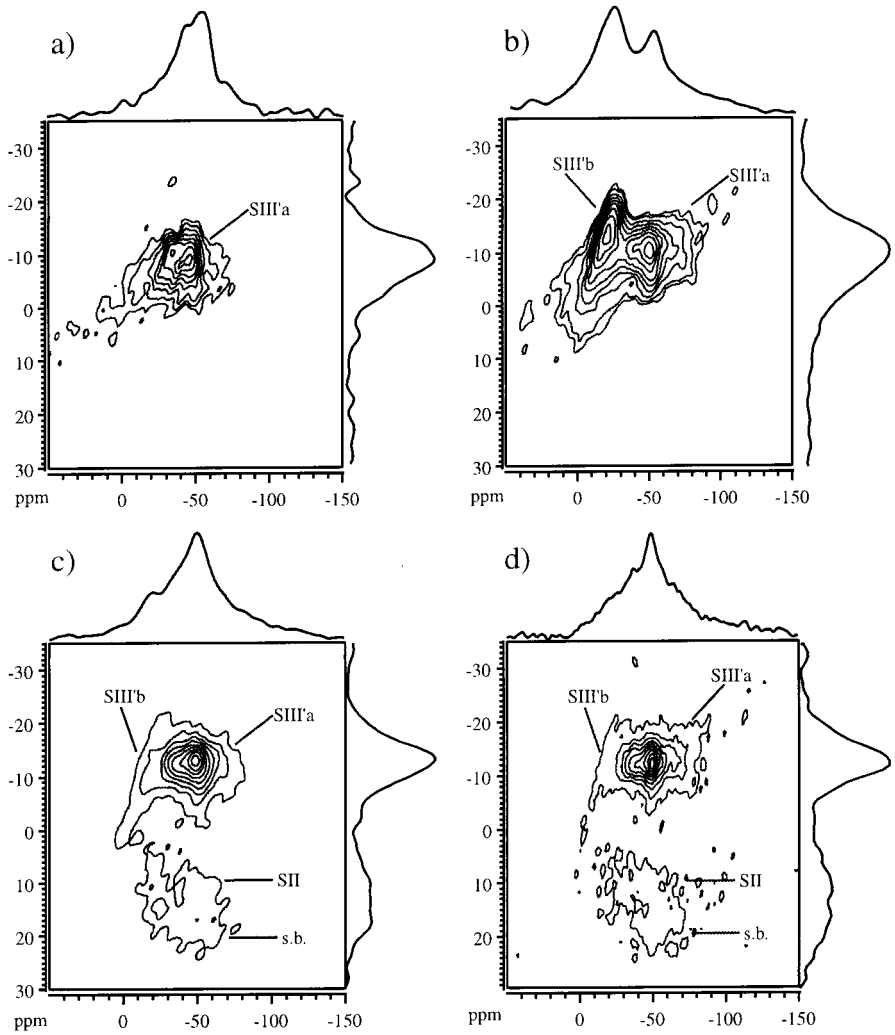

Figure 6. ^{23}Na MQMAS NMR spectra for (a) mixed lithium−sodium chabazite containing 24% sodium, (b) mixed lithium−sodium chabazite containing 39% sodium, (c) mixed lithium−sodium chabazite containing 80% sodium, and (d) pure sodium chabazite. The projection of the anisotropic (MAS) dimension is at the top; the projection of the isotropic dimension to the right. The different sodium sites are identified in the spectra; s.b. designates a spinning sideband.

chosen for the MAS spectra (Figure 5) are fairly consistent with the extracted MQMAS parameters (see Supporting Information) and were further refined using the difference spectroscopy approach. The isotropic chemical shifts and quadrupolar couplings, as well as the cation site populations derived from the MAS spectra, are listed in Table 5.

The ^{23}Na MAS spectra of the two lowest sodium content chabazites, 14 and 24% Na, respectively, have identical line shapes describing the SIII′a site. While this line shape is probably the result of a distribution of asymmetry parameters, a satisfactory simulation can be achieved by assuming two quadrupolar-broadened spectral components having rather similar C_Q but distinct η values of 1.0 and 0.4, respectively. At a sodium content of 39%, the disordered feature discussed above and attributed to SIII′b becomes evident. The MAS spectrum can be simulated using the line shapes from the lower sodium content chabazite with the addition of a broad Gaussian curve simulating the second feature. The use of the distribution is validated by the MQMAS spectra, which clearly show a chemical shift distribution for this species (see above). The spectra for the higher sodium content chabazites were simulated using the parameters from the lower sodium content spectra with the addition of a second-order quadrupolar MAS line shape to simulate the quadrupolar line shape of the SII site ($C_Q = 5$ MHz) observed in the MQMAS spectra.

Discussion

The lithium positions in the lithium form of chabazite are very similar to the sites observed in the various synthetic faujasites, LSX, X, and Y. The lithium SII cation site is fully occupied which is to be expected because the coordination environment is the best available in chabazite for a small cation. Full or near full occupancy has also been observed in the analogous site of lithium faujasite. The SIII lithium cation site in chabazite where the cation coordinates to the side of the channel as opposed to the pore window, has also been observed in some lithium faujasite structures.[3−5] The ^{7}Li MAS NMR spectra correlate well with the diffraction results. The ratio of intensities of the NMR peaks almost precisely matches the population ratios of the cation sites in the neutron diffraction results. Thus the peak at −0.37 ppm results from the SII lithium cations and the peak at −1.2 ppm results from SIII lithium cations. The chemical shift difference between both sites is similar to that observed between SII and SIII sites in lithium faujasites.[5,7] Discrepancies between the cation site populaions derived from MAS NMR and those derived from neutron diffraction have been observed with SIII site type cations.[5] The inconsistent site population from diffraction has been attributed to the effect of a large thermal parameter (U_{iso}) for the site, a result of cation mobility. Since the thermal parameter for the

Table 5. ^{23}Na NMR Simulation Parameters and Site Populations of the Various Mixed Sodium−Lithium Chabazites

	SIII′a	SIII′a	SIII′b[a]	SII	total
100% Na					
δ_{iso} (ppm)	−15.6 ± 1.0	−20.6 ± 1.0	−16.9, σ=15.8	−10.9 ± 1.0	
C_Q (MHz)	4.1 ± 0.2	3.6 ± 0.3	2.0	5.1 ± 0.2	
η	1.0	0.4	−	0.1	
Na^+/u.c	0.89	0.94	0.38	1.32	3.53
9% Li: 91% Na					
δ_{iso} (ppm)	−18.1 ± 1.0	−25.1 ± 1.0	−15.4, σ=11.5	−12.4 ± 1.0	
C_Q (MHz)	3.9 ± 0.2	3.4 ± 0.3	2.0	5.0 ± 0.2	
η	1.0	0.4	−	0.1	
Na^+/u.c	1.18	0.77	0.34	0.92	3.21
20% Li: 80% Na					
δ_{iso} (ppm)	−17.8 ± 1.0	−24.2 ± 1.0	−15.3, σ=15.0	−11.6 ± 1.0	
C_Q (MHz)	4.0 ± 0.2	3.5 ± 0.3	2.0	5.1 ± 0.2	
η	1.0	0.4	−	0.1	
Na^+/u.c	1.41	0.41	0.54	0.46	2.82
58% Li: 42% Na					
δ_{iso} (ppm)	−18.3 ± 1.0	−23.8 ± 1.0	−17.1, σ=9.5	−	
C_Q (MHz)	3.9 (2)	3.4 (3)	2.0		
η	1.0	0.4	−		
Na^+/u.c	0.90	0.43	0.15	0	1.48
61% Li: 39% Na					
δ_{iso} (ppm)	−18.6 ± 1.0	−24.9 ± 1.0	−17.6, σ=12.0	−	
C_Q (MHz)	3.9 ± 0.3	3.5 ± 0.3	2.0		
η	1.0	0.4	−		
Na^+/u.c	0.81	0.16	0.41	0	1.38
76% Li: 24% Na					
δ_{iso} (ppm)	−18.8 ± 1.0	−25.6 ± 1.0	−	−	
C_Q (MHz)	3.9 ± 0.3	3.4 ± 0.3			
η	1.0	0.4			
Na^+/u.c	0.43	0.42	0	0	0.85
86% Li: 14% Na					
δ_{iso} (ppm)	−16.7 ± 1.0	−22.0 ± 1.0	−	−	
C_Q (MHz)	3.9 ± 0.3	3.8 ± 0.3			
η	1.0	0.4			
Na^+/u.c	0.28	0.21	0	0	0.49

[a] σ equals full width at half-maximum for chemical shift distribution, see text.

SIII site in lithium chabazite was constrained, the possible effects of motion were reduced allowing a better determination of the site population. The large standard deviations for the thermal parameters of the cation sites make determination of mobility difficult at best and lead to the use of literature values for the mixed-alkali chabazite.

The exchange of lithium cations with a small amount of sodium results in the selective depletion of the SIII lithium cation population (when the ^{7}Li signal areas are scaled to the cation content of the unit cell, the SIII site occupancy is reduced, while the SII site occupancy remains constant.) In agreement with this result, the ^{23}Na MQMAS spectra of samples containing up to 24% sodium of the cation inventory show only the SIII′ site to be occupied. Although a distribution of η is probably present, the feature is attributed to one crystallographic site. The η distribution is probably related to the disordered nature of the aluminum substitution in the tetrahedral position and the resulting effect on the charge of the framework oxygen atoms coordinating with the sodium cations. The corresponding C_Q value, ∼3.7 MHz, is too small to be from a cation in a highly symmetric planar site like the SII site; sites of this type yield C_Q values on the order of 5 MHz in zeolites such as faujasite and sodalite.[28−30]

Increasing the sodium fraction beyond 24% places additional sodium cations into the channel, populating the disordered SIII′b site. The MQMAS data for the 39% Na sample still does not reveal the presence of Na^+ cations in SII. At this level of sodium exchange, the ^{7}Li MAS spectra reveal that the occupancy of the SII site has only begun to decrease by a small amount, whereas the lithium cations in the SIII sites have been mostly exchanged for sodium. The structure of the 58% Li:42% Na chabazite derived from the neutron diffraction data presents a similar picture. In that model, a clear distinction is visible between the positions of lithium and sodium cations. The neutron diffraction results present the SII site as being exclusively occupied with lithium cations. Sodium cations are positioned in the channel but lie much closer to the eight-ring window than the SIII lithium cations in lithium chabazite. The Na^+ cations are not actually in the window but lie slightly outside the plane of the window. This position is very similar to what has been observed in sodium forms of LSX and X in that the cation sits in the window of the channel as opposed to the cage.[20,31] Such sites have been designated as SIII′ in faujasite and this designation is also used here.

Only at high sodium content does the SII site become occupied by sodium cations. At 80% Na substitution, the MQMAS spectrum shows a low intensity peak with a C_Q value of 5.1 MHz. Line shape simulations of the ^{23}Na MAS spectra also reveal the presence of this sodium site. At this level of sodium exchange, the few lithium cations that remain reside only at the SII site. In the full sodium form, the SII site is more visible in the MQMAS and MAS spectra. However, even at 100% sodium content, the SII site is not completely occupied. On the basis of the MAS spectra, 39% of the sodium cations are found to reside in the SII site, yet this amounts to only 1.4

(28) Koller, H.; Engelhardt, G.; Kentgens, A. P. M.; Sauer, J. *J. Phys. Chem.* **1994**, *98*, 1544−1551.
(29) Engelhardt, G.; Hunger, M.; Koller, H.; Weitkamp, J. *Stud. Surf. Sci. Catal.* **1994**, *84*, 421−428.
(30) Feuerstein, M.; Hunger, M.; Engelhardt, G.; Amoureux, J. P. *Solid State Nucl. Magn. Reson.* **1996**, *7*, 95−103.
(31) Vitale, G.; Mellot, C. F.; Bull, L. M.; Cheetham, A. K. *J. Phys. Chem. B* **1997**, *101*, 4559−4564.

Table 6. SII and SIII′b Site Populations at Various Sodium−Lithium Compositions

composition	SII−Li^+	SII−Na^+	SIII′b−Na^+	total
100% Li	2.22	0	0	2.22
76% Li:24% Na	2.01	0	0	2.01
61% Li:39% Na	1.88	0	0.41	2.29
58% Li:42% Na	1.85	0	0.15	2.00
20% Li:80% Na	0.71	0.46	0.54	1.71
9% Li:91% Na	0.32	0.92	0.34	1.58
100% Na	0	1.32	0.38	1.70

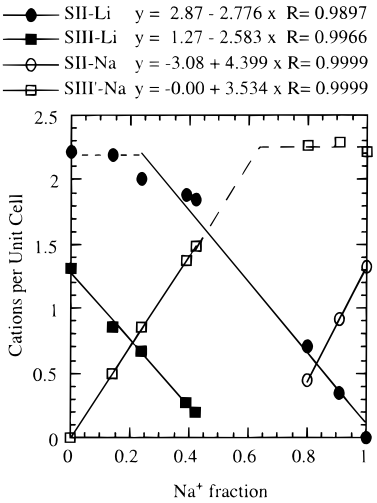

Figure 7. Plot of the sodium and lithium occupancies in mixed-alkali chabazite as a function of sodium fraction. The slopes and intercepts of the linear least-squares fits are listed at the top.

cations per unit cell, corresponding to an occupancy of 70%. Incomplete occupation of the SII site in natural sodium chabazite was also observed by Mortier.[8] In that case, the remaining sodium cations also occupied eight-ring window sites.

The partial occupation of the SII site at high sodium content may explain the broad SIII′b feature that is observed in the NMR spectra. Neutron diffraction results suggest that only one sodium cation site exists in the eight-ring window. However, clear spectroscopic evidence exists for a second sodium environment which is a minority species—never comprising more than 0.5 cations per unit cell. The first appearance of the disordered SIII′b cation environment, at 39% Na content, coincides with a noticeable decrease in the SII lithium site occupation. With higher sodium content, the population of the disordered SIII′b site does not change greatly. Note that the population of this site seems to equal the value of the missing cation population for the SII site in the higher sodium content samples such that the total number of cations occupying the SII site and the SIII′b site never exceeds the crystallographic limit of 2, within the error of the population data derived from the MAS NMR spectra (Table 6). We therefore suggest that the deficiency in the SII site occupation allows for disorder in the SIII′ site. This idea is supported by the fact that the disorder arises only in those samples where the SII site occupancy has decreased significantly below 100%. Such disorder, whether static or dynamic, would be hard to detect with diffraction methods since only a small number of cations are affected.

Figure 7 summarizes the overall results from the population analysis. The increases and decreases of cation populations as a function of sodium and lithium contents show linear trends. Both the lithium SII site and the sodium SIII′ site have population plateaus with the lithium plateau being equal to the maximum occupancy constrained by crystallography. The

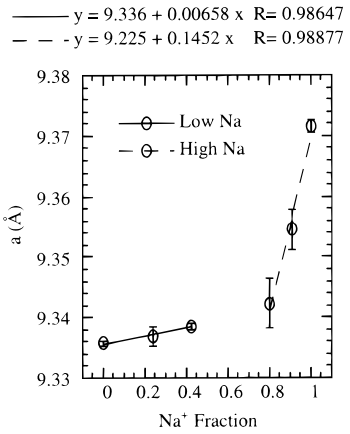

Figure 8. Plot of the lattice constant a in mixed-alkali chabazite as a function of sodium fraction. The change in the lattice constant was fit using two linear functions. The slopes and intercepts of the linear least-squares fits are listed at the top.

sodium SIII′ site (comprising both SIII′a and SIII′b) reaches its population plateau at 63% sodium content; this value is extrapolated from the linear growth observed at lower sodium content. It agrees well with the sodium fraction at which the SII site would begin to be occupied, extrapolated from the observed linear growth curve at the high-sodium end in Figure 7. Thus the occupation of the sodium SII site only occurs after the occupancy at the SIII′ site has reached a maximum value.

The effect of cation site selectivity should manifest itself in the nitrogen adsorption properties of chabazite. Ideally adsorption will occur at the more accessible of the two lithium sites—SIII.[32] Significant improvements in adsorption would be expected when the SIII site is at least partially occupied. On the basis of Figure 7, such improvements are thought to occur at lithium cation fractions above 50%. Such an effect has been observed in chabazite with silicon-to-aluminum ratios between 2.1 and 2.8 where the lithium fraction was at least 65%.[33]

The effect of the different lithium and sodium cation contents is not limited to the cation site locations. The lattice constants of chabazite also change as a function of the cation inventory. The change in the length of the unit cell edge, *a*, is displayed in Figure 8. The change in the lattice constant *a* is not monotonic, but rather consists of two linear regimes with markedly different slopes. The intercept of the two lines occurs at 80% sodium content, which is close to the concentration at which the SIII′ sodium cation population has plateaued and the SII sodium cation population begins to grow. Apparently, this process drives the change in the zeolite framework to form an arrangement in which the bond distances at the SII site now become favorable to sodium cation occupation. From this correlation it is clear that selective siting of the sodium results not from just simple bonding preferences but also from the cooperative interaction of the lattice and the cations in the eight-ring channel.

Conclusions

Lithium and sodium cations demonstrate a definite preference for different cation sites in the zeolite chabazite. Lithium cations prefer coordination at the SII site of the six-ring window. Sodium cations tend to coordinate at the eight-ring window of the channel system of chabazite (SIII′ site). Lithium cations in

(32) Smudde, G. H., Jr.; Slager, T. L.; Coe, C. G.; MacDougall, J. E.; Weigel, S. J. *Appl. Spectrosc.* **1995**, *49*, 1747−1755.

(33) Coe, C. G.; Gaffney, T. R.; Srinivasan, R. S. U.S. Patent 4,925,-460, 1990.

the channel occupy a different position along the four-ring of the hexagonal prism. Magic angle spinning experiments assisted by multiple-quantum NMR spectroscopy can effectively deconvolute the various sodium sites in a zeolite, based on quadrupolar coupling constants, giving a good general picture of the types of sites present in the zeolite. The combined MAS/MQMAS approach is especially effective when the MAS spectra suffers from severe overlap of all the NMR lines present in the sample. Nevertheless, powder diffraction remains essential to quantifying the occupancies and the coordination environments of the cation sites in zeolites. The combined use of both methods has served to give an unambiguous picture of cation siting in chabazite and should prove useful with other zeolites.

Acknowledgment. This work was supported by the United States Department of Energy under Grant No. DE-FG03-96ER14672. Financial support was also provided by the Wissenschaftministerium Nordrhein-Westfalen and by Air Products and Chemicals, Inc. We acknowledge the support of the National Institute of Standards and Technology, U. S. Department of Commerce, in providing the neutron research facilities used in this work. We thank Dr. Tom Gaffney for useful discussions. Experimental assistance by Dr. Brian Toby (NIST) is also gratefully acknowledged. L.S. thanks the Deutsche Akademischer Austauschdienst (DAAD) for providing travel support.

Supporting Information Available: Tables of bond lengths and angles for lithium chabazite and mixed sodium−lithium chabazite. Elemental analysis data for the mixed cation chabazites. Table of chemical shift and quadrupolar coupling data from ^{23}Na MQMAS NMR spectra. ^{7}Li MAS NMR spectra of the satellite transitions (PDF). This material is available free of charge via the Internet at http://pubs.acs.org.

JA992882B